Interpretation example of marine CSEM data

Ståle E. Johansen and Tor A. Wicklund, ElectroMagnetic GeoServices as (emgs), Trondheim, Norway
Hans E. F. Amundssen, EPX, Oslo, Norway

This paper discusses how seabed logging (SBL)—a special CSEM technique developed by Statoil—can be interpreted on a standalone basis and integrated with seismic data. We go through interpretation techniques in which geologic reference areas are compared to the target area and introduce a depth-conversion technique that can be used in the initial phase of interpretation. We also explain how depth migration can estimate lateral extent and depth to resistors. Finally we suggest a classification system for SBL anomalies.

All our evaluations were performed on forward-modeled 3D data and geologic models derived from outcrops on Svalbard in the Norwegian Artic. Due to the low-frequency content in EM data, the original models were simplified for SBL modeling. The Svalbard geomodels were also used for advanced forward seismic modeling (Johansen et al., in press) and this seismic model is visualized with the simulated SBL data.

SBL uses a horizontal electric dipole source and an array of receivers on the seabed. The transmitting dipole emits a low-frequency electromagnetic signal both into the seawater column and downward into the subsurface. The array of seabed receivers measures the amplitude and phase of the transmitted signal; the received voltage depends on the resistivity structure of the subsurface. A survey consisting of many transmitter and receiver locations can determine a multidimensional model of the subsurface resistivity, thus indicating whether the subsurface contains a high-resistivity hydrocarbon-saturated layer. Because the main focus of this study is the interpretation of SBL data, we use synthetic 3D data of a known and well-documented geologic model. In this way, we eliminate the subsurface uncertainties that may occur with real data and are able to study the relationship between geomodel and SBL response in detail.

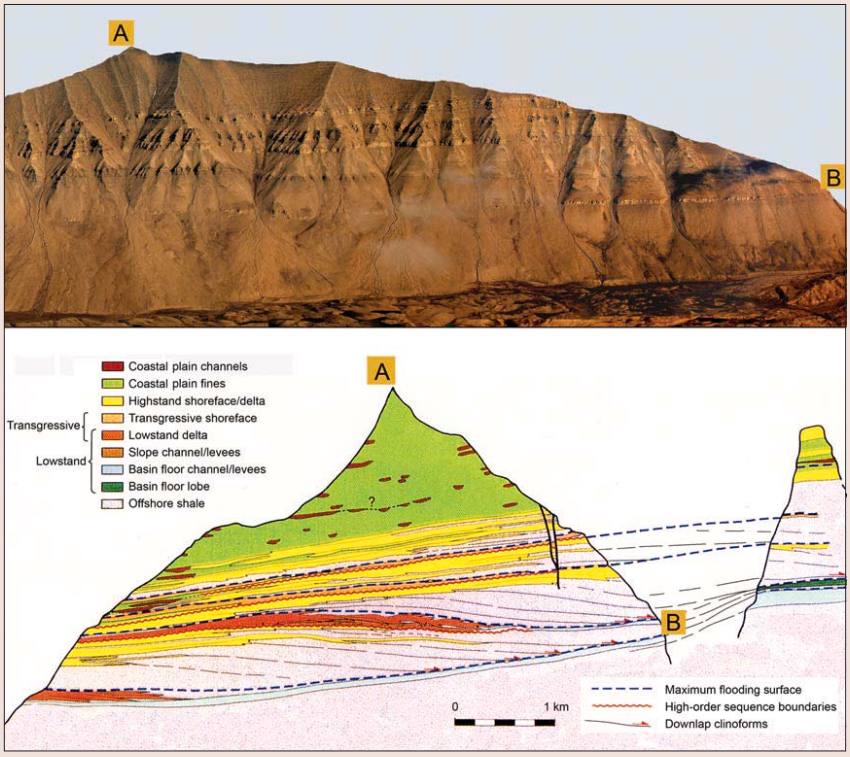

Figure 1. *Outcrops in Van Keulenfjorden, Svalbard in the Norwegian North Sea, and geomodel of the same outcrops.*

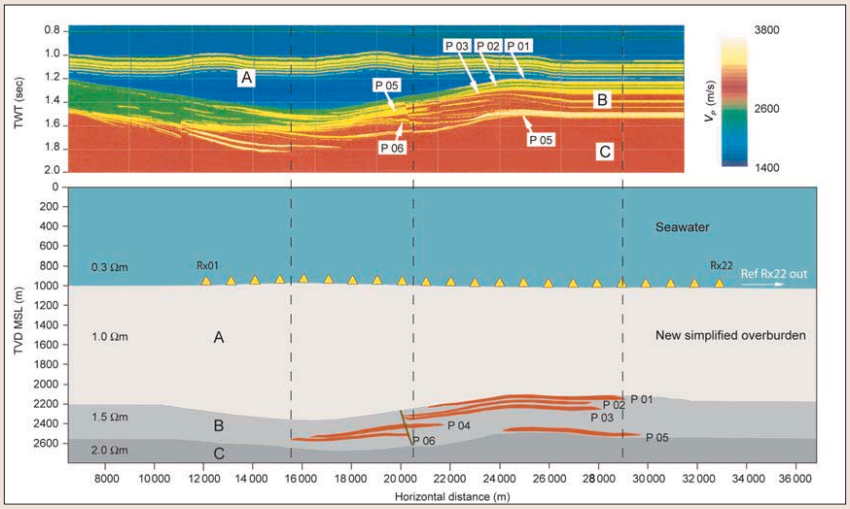

Figure 2. *Geomodel including overburden (from Johansen et al.) and simplified EM model. The resistors are red in the EM model.*

Model and modeling. The geologic model in this study is derived from an integrated outcrop study from Svalbard. The onshore Central Basin of Svalbard is on the main island of Spitsbergen and lines up along a mobile belt that deformed the western margin of the island during Paleogene time. The latest Paleocene-early Eocene infilling of the Central Basin progressed from west to east, and left a spectacular record of large-scale (hundreds of meters), shallow-to-deepwater clinoforms. These are now exposed along the mountainsides reflecting the overall progradation of a coastal plain-delta/barrier shoreline-ramp slope-basin floor sedimentary system. A vertical cross-section of the coastal exposures in Van Keulenfjorden was constructed on the basis of photogrammetry and detailed sedimentological field work. Johansen et al. used this model for forward seismic modeling.

The model used for forward EM modeling is a simplified version of the original geologic model from the integrated outcrop study (Figure 1). Six sandstones were selected for EM modeling, and the background geologic model was divided into three units (Figure 2). The resistivities selected for the background model are based on experience/logs and

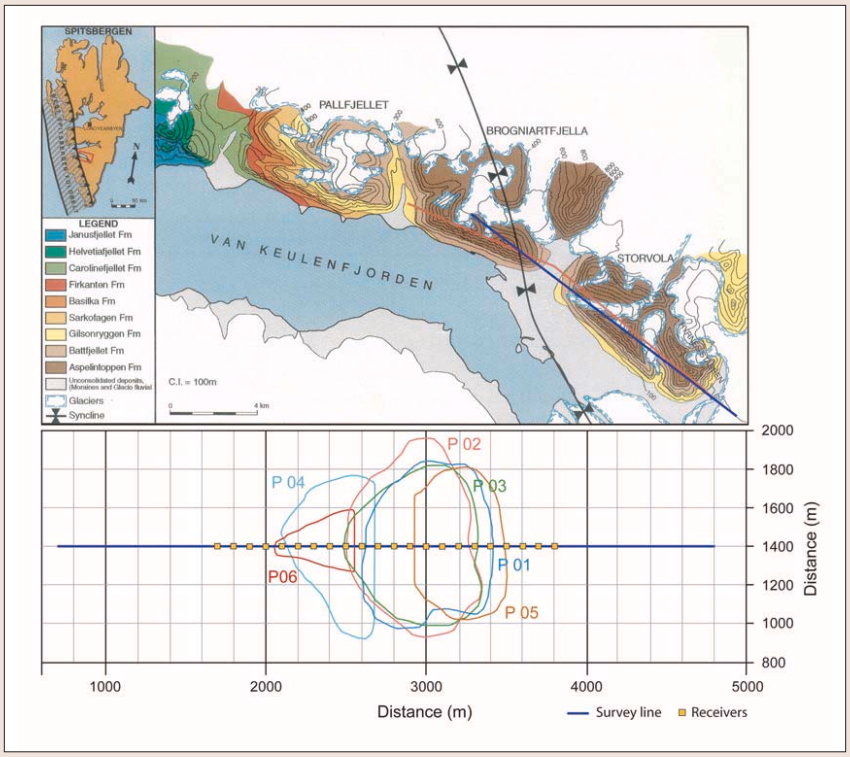

Figure 3. *Prospect outlines, SBL survey layout, and locality map.*

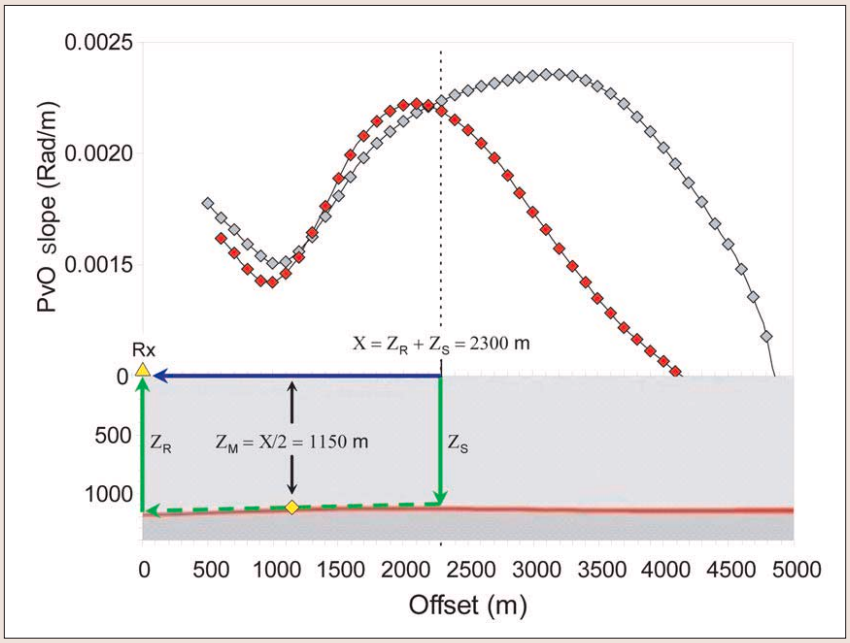

Figure 4. *Depth conversion with apparent depth (AD) method.*

representative of selected passive siliciclastic margins along the Atlantic Ocean. To simulate typical marine acquisition, a 1000-m layer of sea water was added above the geologic model. A water depth of 100 m was also used to study the effect of shallow water. In addition to addressing the effect of shallow water, we interpret the responses from four different georesistivity models. The reservoir sands are hydrocarbon-saturated and combined as shown in Figures 5, 6, 7, and 9. We also simulate a model with an undulating regional buried layer with low resistivity (Figure 10).

The forward modeling code is a 3D FDTD code (Maaoe, 2006) in which Maxwell's equations are solved by approximating partial derivatives with finite differences in the time domain. The solution is found iteratively by time stepping. One significant advantage of using a time-domain code, instead of frequency domain, is that the former requires less memory and is faster. The airwave is included in the forward-modeling code. The method of perfectly matched layers (PML) is used to terminate the electromagnetic fields at the lower and vertical boundaries to avoid artificial reflection back to the computational domain of interest.

The code can handle any source-receiver geometries and computes both horizontal and vertical electric and magnetic fields, with anisotropy if desired. Presurvey feasibility studies, hypothesis testing, and optimizing of survey design are tasks commonly handled through 3D forward modeling. 3D modeling is also very powerful when interpreting SBL data. Additionally, 3D codes are used in inversion and migration (imaging) schemes, as for the migration proposed by Mittet et al. (2005).

Standard processing. The basic processing steps for real SBL data are demodulation, calibration, scaling, and inline rotation. Receiver data are recorded in the time domain. In the demodulation step, time-domain EM data are transformed to frequency domain through a Fourier transform and the frequencies of interest extracted. To relate the recorded signal to the physical field present at the receiver sensors at the time of measurement, the signal is calibrated. After calibration, the recorded data are converted to the EM field quantities. The phase of the source current is used to obtain absolute phase data, meaning that the phase of the E-field is zero at zero Tx-Rx offset. The current amplitude is accounted for through normalization by the dipole current moment. The strength of the electromagnetic field at the antennas depends on their orientation relative to the transmitted field. For any given angle of the receiver sensors, they measure the legs of the total EM vector field. Based on this, the antenna orientation compared to the transmitted field can be determined if the receiver is positioned inline (along the x axis) with the transmitted electromagnetic field (given the source is an x-directed dipole). In this case, the total field will be dominated by the Ex and Hy components (over the Ey and Hx components) and rotation angles computed through maximization of Ex and Hy. The three first steps of standard processing of real data are accounted for in the 3D forward modeling code. The inline rotation is a separate processing step.

Up-down separation and migration. In shallow water (< 300 m), SBL measurements are complicated by downward-propagating components which have been refracted and reflected off the sea surface due to the extreme velocity contrast between conductive sea water and highly resistive air. This phenomenon, known as the airwave, is primarily dominated by energy propagating upward from

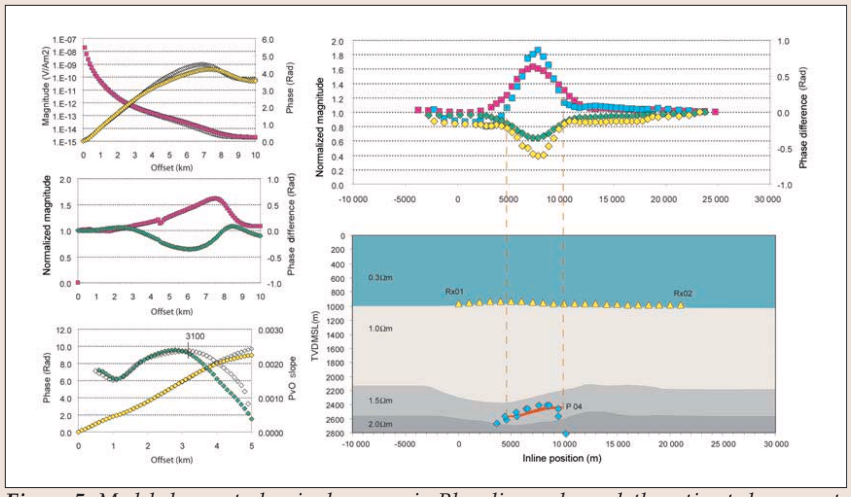

Figure 5. Modeled case study, single reservoir. Blue diamonds mark the estimated apparent depth (AD).

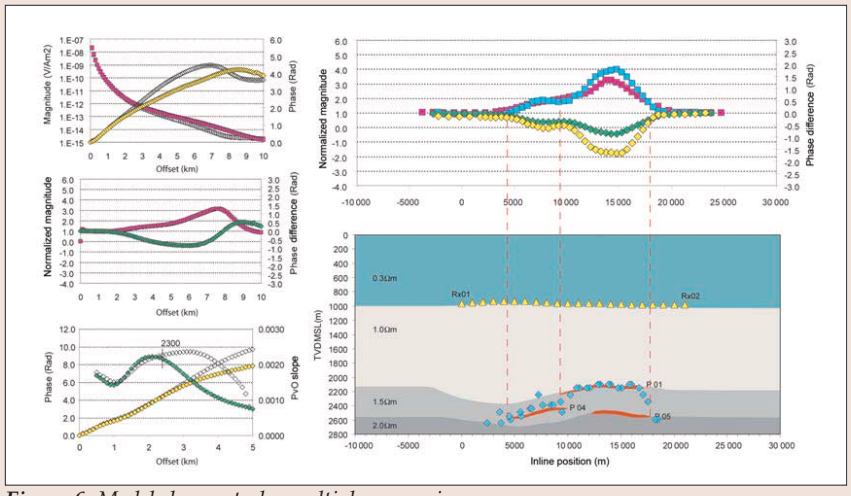

Figure 6. Modeled case study, multiple reservoirs.

the source to the sea surface, laterally along the sea-air interface without attenuation, and down again to the receivers at the seafloor. These downward-propagating fields interfere with upgoing fields from the subsurface and can potentially mask an otherwise significant response from a reservoir—or lead to erroneous interpretation of the data, if not properly accounted for during processing. The source-receiver offset at which the airwave starts to dominate the recordings depends on water depth, frequency, and subsurface resistivity distribution.

Up-down separation is a method to decompose the measured EM fields into upgoing and downgoing components (Amundsen et al., 2006) and hence remove airwave components and magnetotelluric (MT) noise from the recorded data. In order to decompose the fields, both the horizontal electric and magnetic components are needed. Up-down separation can therefore only be applied to receivers equipped with both electric sensors and magnetic coils.

A more sophisticated way to calculate the vertical and horizontal position of the subsurface resistor is depth migration. Depth migration of SBL data can be compared to wave-equation prestack depth migration of seabed seismic data. In the calculations the elastic wave equation is replaced by Maxwell's equations. The depth resolution of an SBL survey is much lower than that of a seismic survey and a typical SBL frequency range is 0.1–3.0 Hz. Imaging techniques used in seismic depth migration correlate up- and downgoing waves and assume reflection from impedance contrasts. This assumption is not well suited for EM energy guided by a resistive formation. By modifying the standard imaging condition and introducing a nonlocal imaging operator, the accuracy of the vertical and the horizontal positioning of the resistor improves. See "Explicit 3D depth migration with constraint operator" by Mittet (GEOPHYSICS, 2006) for details on depth migration of SBL data.

The input required for the migration is the transverse resistance (thickness times resistivity) of one or several resistors and a background resistivity versus depth model. The latter is normally derived from plane-layer inversion of off-target reference receivers. The output from the migration is lateral extension and the calculated depth to the subsurface anomalies.

Interpretation. SBL surveys allow remote sensing of subsurface resistivity contrasts. Subsurface resitivities are controlled by permeability, pore space geometry, and pore fluid composition. While water-wet sediments generally have resistivities in the range 1–5 Ω-m, hydrocarbon-bearing sediments have much higher resistivities of around 10–100 Ω-m.

During an SBL survey, periodic EM energy is continuously generated by a dipole source. The receivers record energy traveling directly from source to receiver, reflected and refracted energy from the subsurface, and reflected and refracted energy from the sea-air interface. If the reservoir resistivity is high due to hydrocarbon saturation, the energy from the subsurface will include guided energy from the reservoir. Depending on source-receiver distance, subsurface structure, and water depth, one of three energy modes will dominate the recorded signal. The "direct energy" will dominate the continuously recorded signal at short source-receiver offsets. As the offset increases, energy from the subsurface will dominate the recorded signal. The offset at which this occurs depends both on subsurface structure and water depth. The energy refracted along the sea-air interface (airwave) will dominate the recorded signal at relatively large offsets. Exactly where depends strongly on the water depth, but also on the strength of returned energy from the subsurface. In deep water (more than about 1500 m), only a minor airwave contribution to the recorded signal is seen for offsets less than 10 km. This contribution increases as the water depth decreases.

Magnitude and phase versus offset. Comparison of magnitude versus offset (MVO) signatures is done by calculating normalized magnitudes relative to a chosen reference receiver. Normalized magnitudes around 1 indicate MVO signatures similar to the reference receiver and no apparent increased magnitude readings due to, for example, subsurface resistivity anomalies. Normalized magnitudes significantly higher than 1 at intermediate to far offsets suggest increased magnitudes due to subsurface resistivity anomalies. Systematic inline variations in MVO are highlighted by monitoring normalized magnitudes at a chosen offset and posting these at "common midpoint" position (i.e., ½ × offset) relative to receivers (summary plot). Normalized magnitudes are sampled as median normalized values, typ-

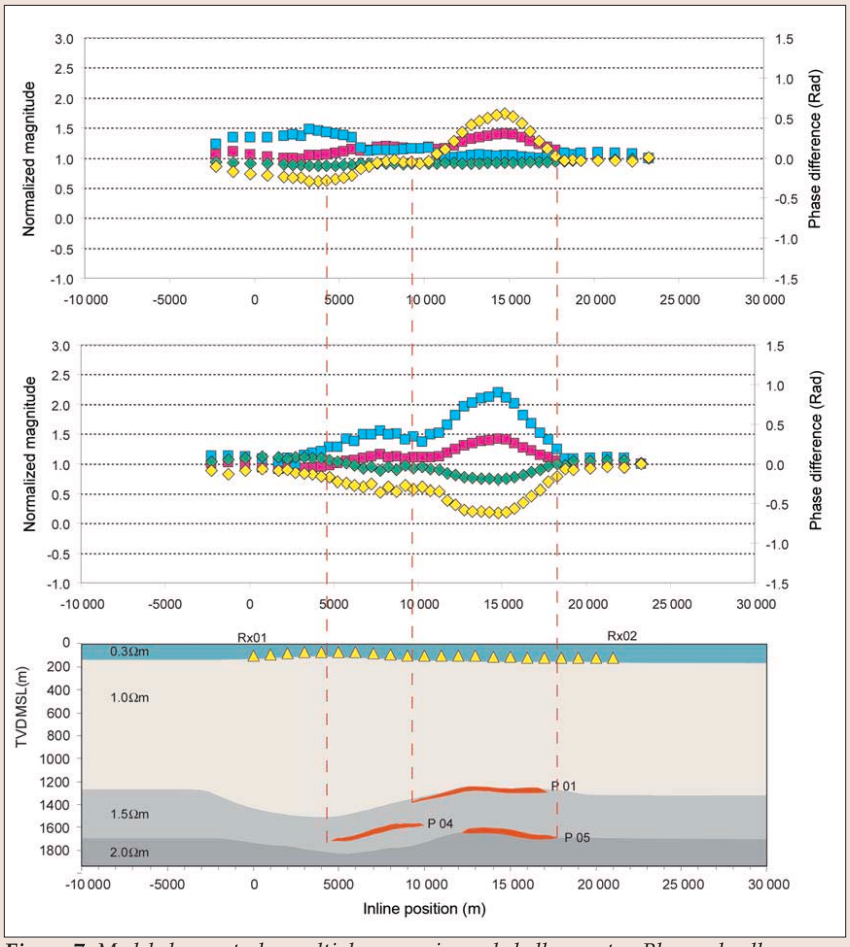

Figure 7. *Modeled case study, multiple reservoirs and shallow water. Blue and yellow colors represent 0.25 Hz while red and green represent 0.05 Hz. The lower panel shows the responses after up-down separation.*

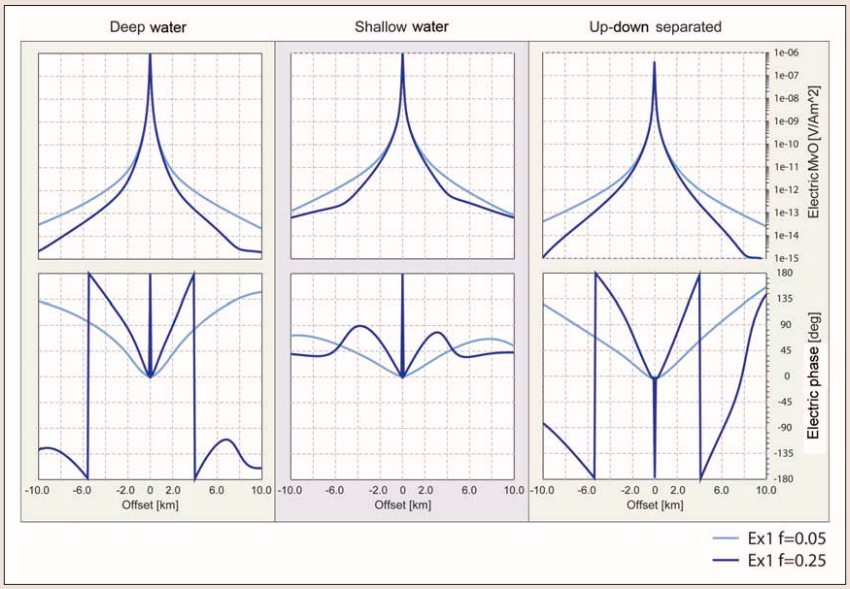

Figure 8. *Electric MVO and PVO for one receiver located close to the edge of a reservoir in a deep and shallow water setting. Airwave removal has been applied to the shallow water data using up-down separation.*

ically within a 1-km offset range to level out noise effects.

Comparison of phase versus offset data (PVO) is done by either calculating phase difference relative to the reference receiver at a given offset or by calculating PVO slopes using a 1-km sliding window. Lower PVO and PSVO values relative to the reference receiver indicate phase shifts due to subsurface resistivity anomalies.

Apparent depth (AD). Based on high-frequency PVO data, we have developed a simple depth-conversion technique. Phase versus offset data for target receivers record decreased $\delta\varphi(x)/\delta x$ relative to reference receivers beyond a certain offset (Figure 4). We assume that this offset represents the distance where the EM signal is transmitted with equal speed subparallel to the seabed and via a subsurface high-resistivity layer (HRL). Assuming that signal traveltimes along the HRL are negligible, the fastest subsurface travel path can be approximated as the vertical distance from the source to the HRL (Z_S) plus the vertical distance from the HRL to the receiver (Z_R). Accordingly, we arrive at a simple relation between the offset X and the mean burial depth to the HRL (Z_M): $Z_M = X/2$.

Modeled case studies. The geomodel in the first, *single-reservoir, interpretation* case (Figure 5) is a 25-m prospect with 50 Ω-m resistivity in the reservoir. The background model resistivity is 1.5 Ω-m. The prospect is a combined structural and stratigraphic trap with a typical shape and size for the shallow marine setting of the prograding package filling in the Central Basin in Eocene times (Figures 1–3). Both electric and magnetic components are available from the modeling but here we chose to base the interpretation on the electric component of the field. The anomaly in the 1.25-Hz summary plot correlates reasonably well with the extension of the prospect, and the maximum amplitude is above the center of the reservoir. The relative increase in return energy compared to the reference area (out-towing receiver 22) is close to 90%. The increase in amplitude correlates with the increase in transverse resistance (thickness times resistivity) of the prospect area compared to the reference area. The phase difference (lower curve) confirms the amplitude anomaly. The phase difference is proportional to the EM velocity increase in the prospect area compared to the reference area. The AD analysis gives a depth to the reservoir that correlates with the actual reservoir depth. The prospect dip is resolved by the AD method in this case. On the 0.25-Hz signal, the response is more smeared out and the summary plot response does not correlate as well with the edges of the prospect. A regional change in background resistivity is also seen in the summary plot with lower readings on the in-towing (left) side of the prospect. This correlates with the syncline in the background model.

To analyze a case with *multiple reservoirs* (Figure 6), we have added two more reservoirs from the general model. The upper one is a shallow marine combined structural-stratigraphic trap while the lower trap is a basin floor fan.

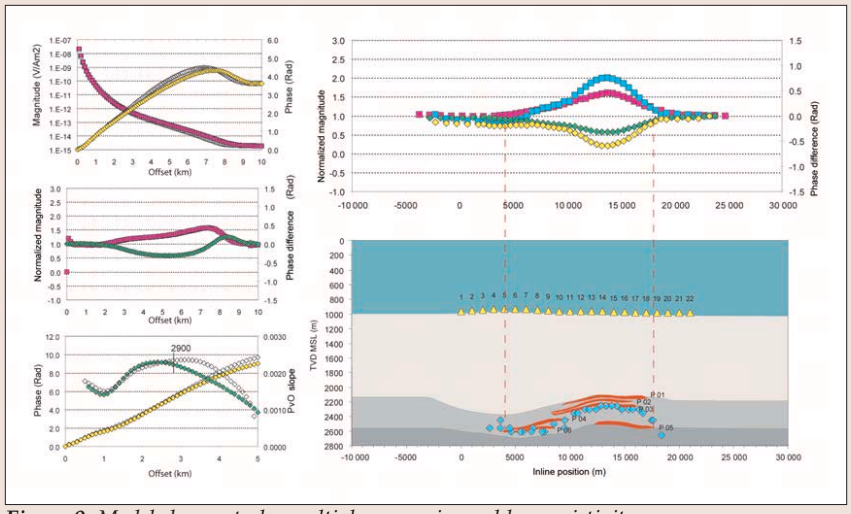

Figure 9. *Modeled case study, multiple reservoirs and low resistivity.*

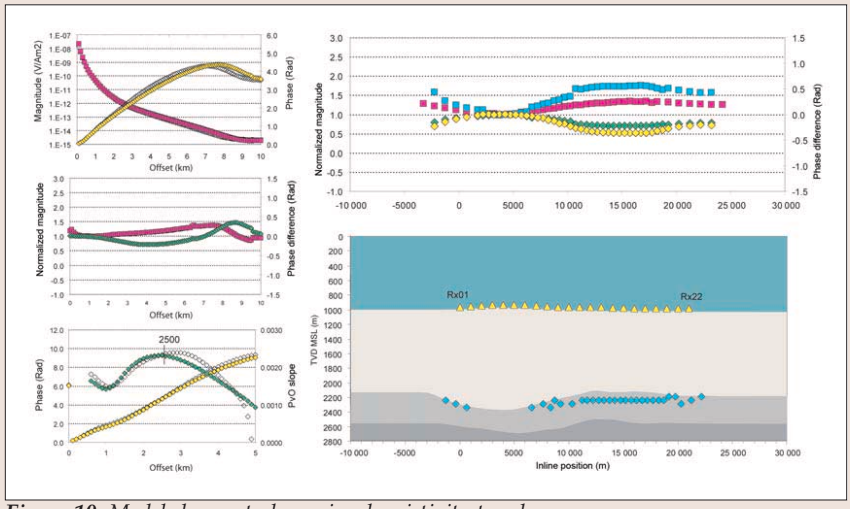

Figure 10. *Modeled case study, regional resistivity trend.*

When more resistors are added in the subsurface, the EM response at the surface increases on both frequencies. The summary plot shows a very clear step behavior with a significant increase in return energy above the stacked doubled reservoir. We also see how the phase curve records the gap between the two lower reservoirs. The AD analysis gives a depth that correlates well with the top of the reservoir zone. This simple analysis cannot handle stacked reservoirs. However, the eastern edge of the upper reservoir is well defined by this technique. This case is further discussed below.

To understand how *shallow water* depth will influence the interpretation of the SBL data, we have replaced the 1000-m water layer in the previous case with a 100-m water layer. The rest of the model is identical (Figure 7). The effect of the water layer dramatically changes the SBL response. Strong influence from the water layer creates a new and complex response and a phase and magnitude crossover is created in the 0.25-Hz case. However, two techniques can improve the understanding of the subsurface response in shallow water. Figure 8 illustrates how the airwave is "pushed" to higher offsets when the frequency is lowered. The problem with this approach is that a large prospect is needed to get a response from the subsurface. Here it works, but the summary plot shows that the amplitude resolution is low and that the recorded phase change from reference area to prospect area is negligible. It is also possible to reduce the shallow water effects by performing up-down separation on the data (Figure 8). This increases the amplitude resolution and especially the phase response for both the 0.05-Hz case and the 0.25-Hz case.

Occasionally the *resistivity in the reservoir is low*, and this is a potential problem for the SBL method. In this case we simulate a case with stacked reservoirs with low-resistivity "pay" (Figure 9). When the resistivity is as low as 8 Ω-m, the response is very sensitive to the background resistivity. When acquiring data in such a setting, it is critical to collect data on all sides of the prospect to understand changes in the regional resistivity. To secure reliable SBL results, it is now standard to acquire data in a grid pattern when dealing with low-resistivity targets. The AD analysis gives a reasonable depth estimate for this low-resistivity case but the exact behavior of this method with multiple reservoirs is uncertain. The return energy increased by 60% in the 0.25-Hz case and up to 100% in the high-frequency case. The background model interferes with the reservoir model with an imprint of the syncline especially in the 1.25-Hz case. We should also keep in mind that the total resistor volume is large in this case.

In the final case (Figure 10), we have replaced all reservoirs with an *undulating regional stratigraphic layer* with a resistivity of 3.8 Ω-m. Accounting for the effect of such an undulating layer in combination with thickening and thinning effects is important in SBL interpretation. Here the receiver with lowest reading is used as reference receiver, and the increase in response is frequency-dependent and varies between 30 and 65%. Also in this case AD analysis gives an estimation of depth to the resistor, but we also see a slope curve crossover in this case. This indicates a setting in which the AD method should be used with caution. We also see that the magnitude and phase anomalies never close laterally. This is often the case for regional anomalies. When evaluating the nature of SBL anomalies, the gradient of the amplitude and phase summary curves will help distinguish regional from more local anomalies.

Depth migration and integration for the multiple reservoir case. For proper calculation of vertical and horizontal position of resistors, migration or inversion is needed. Here we have chosen to migrate the SBL data and integrate the results with the other geodata. The result is shown in Figures 11 and 12. This illustrates very clearly the difference in resolution between EM data and seismic data. The migrated depth is measured in the middle of the anomaly and for the single reservoir the migrated depth and the real depth are almost equal. Also, for the double reservoir, the migration gives a good result as the migrated depth is between the two reservoirs' depths. The lateral extension of the reservoirs is also well spotted by the migration. However, the migration can, in this case, not identify the two stacked reservoirs, but suggests that the resistor volume increases toward the east (right). The AD analysis gives additional information which indicates very well the depth to the single resistor (left) and to the upper resistor (right). It also con-

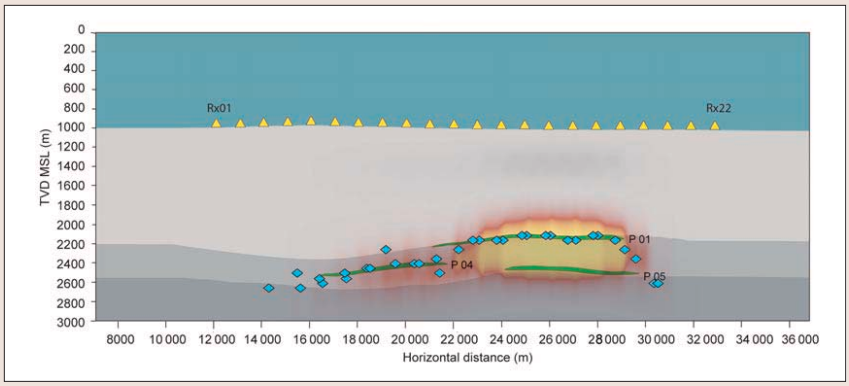

Figure 11. *Integration of geomodel, AD analysis depth and migrated data from the multiple reservoir case in Figure 5.*

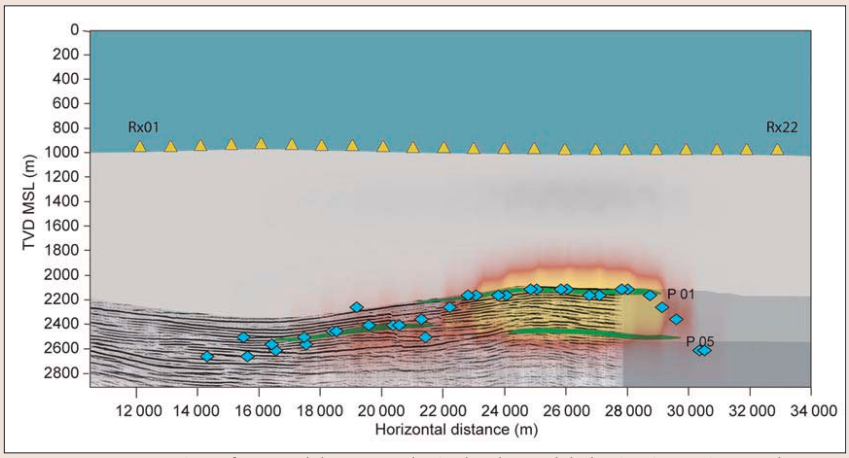

Figure 12. *Integration of geomodel, AD analysis depth, modeled seismic section, and migrated data from the multiple reservoir case in Figure 5.*

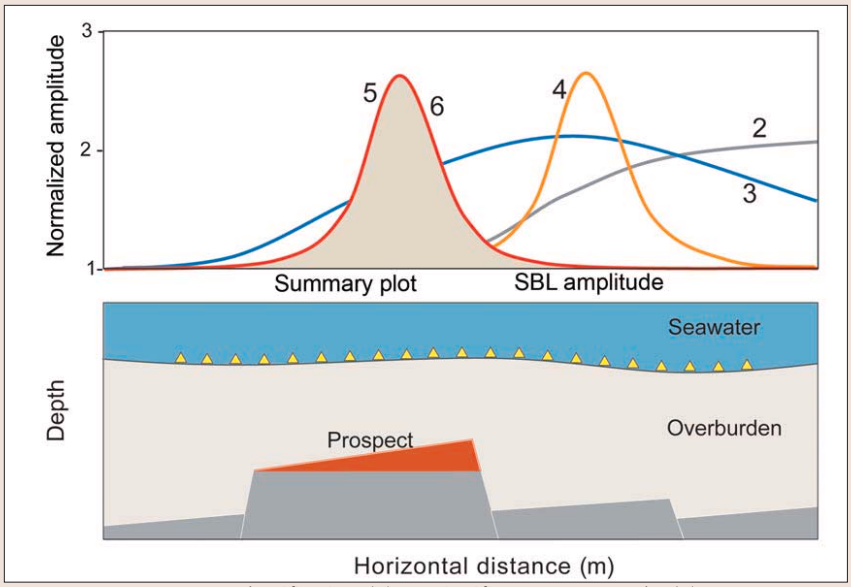

Figure 13. *SBL response classification. (1) No significant SBL anomaly, (2) open SBL anomaly outside prospect, (3) open SBL anomaly partly over prospect, (4) closed SBL anomaly outside prospect, (5) closed SBL anomaly over prospect with antimodel, and (6) closed SBL anomaly over prospect.*

firms the lateral extension of the upper resistor in an easterly direction.

If we now compare the geodata in Figure 1 with the results in Figure 12, we see both the seismic and SBL response of the original geologic model. The uppermost sandstone in Figure 1 corresponds to the upper green reservoir in Figure 12, and the lowermost sandstone correlates with the lowermost green reservoir. The reservoir sandstones in the outcrop have a thickness of 20–30 m and can be "buried" to a considerable depth and still be visible on SBL data. The seismic image of the buried reservoirs is much more detailed than the SBL response of the same strata, but as shown by Johansen et al., it is also much more complex. It is difficult to map out the present sandstones and to define structural and stratigraphic prospects in this setting. Further, to decide which of the mapped reservoirs contain hydrocarbons is, of course, extremely challenging. The stratigraphic traps in the eastern portion of the seismic section are really challenging. SBL measures a different parameter from seismic and can detect the high-resistive bodies in the subsurface independently from seismic. But the combination of electric and acoustic measurements is much more powerful than seismic alone.

Classification of SBL responses. To evaluate and compare SBL responses we suggest a simple classification system. In Figure 13 we have defined six amplitude summary plot categories. The two highest categories are SBL responses that correlate with the subsurface target. If there are antimodels in the prospect area, the rating is generally reduced. Antimodels are resistors that are explained by nonhydrocarbon subsurface bodies such as volcanic intrusives, tight lithologies (basement), or evaporites. Often anomalies occur outside the defined target. Such anomalies are classified as an anomaly at level 4, but the anomaly can be upgraded by seismic mapping. If the anomaly only partly correlates with the target, it is classified at level 3. At level 2 the anomalies do not close and are outside the target area. If there is a very weak or no SBL response above a target, this anomaly is classified at the lowest level.

The models from Svalbard are easy to classify because all the anomalies correlate and close above their respective targets. The only exception is that the regional case would be classified as category 2 or 3 depending on how the prospect was defined. In Svalbard, the shallow basement and intrusives are obvious antimodels that could lower the classification level of the observed SBL anomalies. This classification system is not limited to single lines, but could also be used on a more general basis. Finally, how such a classification system could be used in prospect evaluation is of course up to the individual oil company to decide.

Suggested reading. "Reservoir analog studies using multimodel photogrammetry: A new tool for the petroleum industry" by Dueholm and Olsen (AAPG *Bulletin*, 1993). "Sedimentation in a Paleogene foreland basin, Spitsbergen" by Helland-Hansen (AAPG *Bulletin*, 1990). "Geometry and facies

of Tertiary clinothems, Spitsbergen" by Helland-Hansen (*Sedimentology*, 1992). "Subsurface hydrocarbon detected by electromagnetic sounding" by Johansen et al. (*First Break*, 2005). "Decoupling of seismic reflectors and stratigraphic timelines: a modeling study of Tertiary strata from Svalbard" by Johansen et al. (GEOPHYSICS, in press). "Tertiary stratigraphy and tectonism in Svalbard and continental drift" by Kellog (AAPG *Bulletin*, 1975). "Fluvially incised shelf-edge deltas and linkage to upper slope channels (Central Tertiary Basin in Spitsbergen)" by Mellere et al. (in *Global Significance and Future Exploration Potential, Special Publication GCS-SEPM*, 2003). "Fast finite-difference time domain modeling for subsurface electromagnetic problems" by Maaoe (*SEG 2006 Expanded Abstracts*). "Decomposition of electromagnetic fields into upgoing and downgoing components" by Amundsen et al. (GEOPHYSICS, 2006). "Remote reservoir resistivity mapping" by Srnka (*TLE*, 2006). "Marine electromagnetic methods—a new tool for offshore exploration" by Constable (*TLE*, 2006). "Deltas versus rivers on the shelf edge: their relative contributions to the growth of shelf-margins and basin-floor fans (Barremian and Eocene, Spitzbergen)" by Steel et al. (*SEPM Special Publication, 28*, 2000). "Clinoforms, clinoform trajectories, and deepwater sands" by Steel and Olsen (in *Sequence Stratigraphic Models for Exploration and Production, GCS-SEPM Special Publication*, 2002). "Sea bed logging (SBL), A new method for remote and direct identification of hydrocarbon filled layers in deepwater areas" by Eidesmo et al. (*First Break*, 2002). "Remote sensing of hydrocarbon layers by seabed logging (SBL): Results from a cruise offshore Angola" by Ellingsrud et al. (*TLE*, 2002). "A two-step approach to depth migration of low frequency electromagnetic data" by Mittet et al. (*SEG 2005 Expanded Abstracts*). TLE

Acknowledgments: We thank emgs for the permission to publish this paper. We also thank our colleagues in emgs for valuable help and critique. Special thanks to Stig Arne Karlsen for excellent graphical work.

Corresponding author: sj@emgs.com